

# Antiprotonic studies of nuclear neutron haloes

S. Wycech<sup>\*</sup>, J. Skalski<sup>†</sup>, and R. Smolańczuk<sup>‡</sup>  
*Soltan Institute for Nuclear Studies, Hoża 69, PL-00-681, Warsaw, Poland*

J. Dobaczewski<sup>§</sup>  
*Institute of Theoretical Physics, Warsaw University, Hoża 69, PL-00-681, Warsaw, Poland*

J.R. Rook  
*Particle and Nuclear Physics Laboratory, University of Oxford*

Nuclear capture of antiprotons from atomic states is studied. Partial widths for single nucleon capture events leading to cold residual nuclei are calculated. Recent CERN experiments that compare the neutron and proton captures are analysed. Nuclear density distributions at extreme nuclear surface are calculated and tested against the experimental results.

## I. INTRODUCTION

Recent CERN experiments with antiprotonic atoms [1] have renewed interest in the question of the comparison of the proton and neutron density distribution at the surface of large nuclei. It has been known for years that hadronic, in particular kaonic atoms, provide a way to study the extreme tail of the nuclear density distribution, its isospin structure and nuclear correlations there [2]. Two methods have been used [3–9], each of which gives information in the region roughly 2.0 fm beyond the half density radius.

1) An observation of the X-ray cascade in hadronic atoms and extraction of the atomic level shifts and widths. These level widths, related to the nuclear absorption of hadrons may determine high moments of the nuclear density distributions. Information obtained in this way is rather limited, however. For a given atom only one, and in some special cases two level widths and one level shift, can be measured. The latter is in general difficult to interpret and provides a check on the hadron-nucleon interaction models.

2) Studies of the nuclear absorption products in particular detection of the emitted mesons. In this way one can discriminate captures on protons from captures on neutrons. In principle, more nuclear information is offered but it is also more difficult to interpret. The reason is that the initial states of capture are not known directly and the final mesons may exchange charge or become absorbed.

---

<sup>\*</sup>Internet address: WYCECH@FUW.EDU.PL

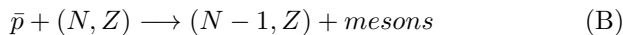
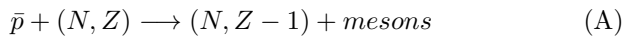
<sup>†</sup>Internet address: JSKALSKI@FUW.EDU.PL

<sup>‡</sup>Internet address: SMOLAN@FUW.EDU.PL

<sup>§</sup>Internet address: DOBACZEW@FUW.EDU.PL

The new experiments of Ref. [1], involving antiprotons, have two very strong advantages. Firstly they differentiate reasonably clearly between the  $\bar{p}p$  annihilations and  $\bar{p}n$  annihilations, thus ensuring that the neutron and proton distributions can be separately estimated. Secondly, they involve antiproton absorption very much further from the nuclear half density radius than the earlier experiments mentioned above. We shall show that the absorption occurs around a region 3.0 fm beyond the half density radius.

The idea of the experiments of Ref. [1] is to detect "cold" nuclei, following the absorption of antiprotons in antiprotonic atoms, by radiochemical methods. By "cold" here we mean nuclear states of very low energy, less than the neutron emission threshold. Characterising a nucleus of  $N$  neutrons and  $Z$  protons by  $(N, Z)$  the reactions are



Thus (A) involves predominantly interactions of the  $\bar{p}$  with protons and (B) similarly with neutrons. It is this feature which is the first advantage of this method mentioned above.

The extreme surface nature of the process arises firstly from the high orbital angular momentum of the  $\bar{p}$ , but this is well known and is exploited in the earlier experiments [3-9]. However the new feature, giving increased surface emphasis arises from the mesons in (A) and (B). On average there are 4-5 mesons emitted and to leave a "cold" nucleus they must all avoid hitting the nucleus. This can only be achieved in the far surface.

The basic  $N\bar{N}$  interactions required for this study are limited by several phenomenological parameters - range of the  $N\bar{N}$  annihilation, absorptive parts of the scattering amplitudes, pion production multiplicities, pion momentum distributions. These are taken from other experiments while effects of uncertainties must be quantified. Once the final and initial states are under control one can interpret the  $(N - 1)/(Z - 1)$  ratios in terms of "neutron haloes" or "neutron skins" and attribute quantitative meaning to these terms. Qualitatively, the CERN experiments [1] discover large neutron excess at the nuclear surface of several heavy nuclei. It complements similar findings in the subcoulomb neutron pickup reactions [10].

One purpose of this paper is to provide a description of the nuclear capture of the atomic antiprotons. Of main interest is that fraction of single nucleon captures which leaves cold nuclei in the final states. This is the scenario of the recent experiment [1]. Difficulties in the way are twofold. First, the  $N\bar{N}$  annihilation is a complicated process with many degrees of freedom involved. Second, the initial atomic state of the antiproton and the final states of the residual nuclei are not certain. Fortunately, the first difficulty is moderated by a large energy release in the  $\bar{p}$  absorption. Hence, a closure over nuclear final

states and high energy approximations for the annihilation mesons may be applied and these yield classical formulas for the absorption rates. The latter are expressed by integrals of nuclear densities weighted by a probability to find the antiproton inside nucleus and a probability to find the final nucleus left undestroyed by the annihilation products. The last two probabilities are calculated on the basis of the antiproton and pion optical potentials. Their dependence on the initial atomic state, final state interactions and parameters of the  $\bar{p}$  and pionic nuclear optical potentials are studied in Section II.

Nuclear models of various complication: Fermi gas, shell model, Hartree-Fock and Hartree-Fock-Bogolyubow methods are used in Section III to find the nuclear density distributions. Comparison with the experiment is done and dependence on nucleon binding energies, Coulomb barriers, shell structure and correlations is studied. The advantages and limitations of the experimental method are indicated.

## II. NUCLEAR ABSORPTION OF ATOMIC ANTIPROTONS

Antiprotons bound into atomic orbits cascade down to be ultimately absorbed by the nucleus. The latter happens at the extreme nuclear surface and the absorption probability is significant even at distances as large as twice the nuclear radius, [3,8,9]. Two effects create such a situation. First, the free path of antiprotons in nuclear matter is less than 1 fm and second, the atomic cascade tends to populate states of high centrifugal barrier  $l$ . The peripherality of capture allows for standard low density simplifications: quasi-free scattering and single-particle picture of the nucleus. Also, it facilitates the description of the final mesons, a vital question for understanding the absorption experiments. On the other hand the disadvantage and difficulty inherent in the surface studies is related to its sensitivity to range effects.

This section presents a description of the antiproton absorption mechanism. First, a simple phenomenological picture based on the optical potential model is presented. Next, two special questions: final state interactions and range effects are discussed, again in a phenomenological way. A more detailed justification of the phenomenological approach, basic assumptions and limitations are given in two consecutive subsections. These contain rather technical discussion which may be omitted by readers more interested in the nuclear structure results.

The tool to describe the antiprotonic atomic level shifts and widths is an optical potential  $V^{\text{opt}}$ . The simplest one is assumed usually [8,9,11] in the form

$$V^{\text{opt}}(\mathbf{R}) = \frac{2\pi}{\mu_{N\bar{N}}} t_{N\bar{N}} \rho(\mathbf{R}) \quad (1)$$

where  $\mu_{N\bar{N}}$  is the reduced mass,  $\rho(\mathbf{R})$  is a nuclear density at a radius  $\mathbf{R}$  and  $t_{N\bar{N}}$  is a complex scattering length.

As there is some finite range in the  $N\bar{N}$  interaction the density  $\rho(\mathbf{R})$  involved in Eq.(1) is not the "bare" nucleon density  $\rho_0(\mathbf{R})$  but a folded one

$$\rho(\mathbf{R}) = \int d\mathbf{u} \rho_0(\mathbf{R} - \mathbf{u}) v(\mathbf{u}) \quad (2)$$

where  $v$  is a formfactor that represents the  $N\bar{N}$  force range. For the absorptive part of  $V^{\text{opt}}$  the annihilation range of 1 fm might be expected from models of the  $N\bar{N}$  annihilation but the range in the real part is more difficult to control.

The length  $t_{N\bar{N}}$  in Eq.(1) is extracted from antiprotonic atomic data. The most precise X-ray measurements have been done for the 3d and 4f states in the oxygen isotopes, [8,9], and fits to these give  $t_{N\bar{N}}$  of about  $-1.5 - i2.5$  fm, [11,12]. This value yields a deep and strongly absorptive potential well. At the nuclear centre  $\text{Im}V^{\text{opt}}$  would be 200 MeV strong and the related free path length would be well below 1 fm. However, it should be kept in mind that both the form and the strength of  $V^{\text{opt}}$  is tested only in the surface region. In particular,  $\text{Im}V^{\text{opt}}$  is determined by the atomic level widths, via

$$\Gamma = 4 \frac{\pi}{\mu_{N\bar{N}}} \text{Im} t_{N\bar{N}} \int d\mathbf{R} \rho(\mathbf{R}) |\Psi_{\bar{N}}(\mathbf{R})|^2 \quad (3)$$

where  $\Psi_{\bar{N}}(\mathbf{R})$  is the atomic wave function. Since  $\Psi_{\bar{N}} \approx R^l$  and only high angular momenta  $l$  are available, the absorption strength is peaked at the surface.

The nuclear absorption scenario in  $^{58}\text{Ni}$  is visualised in Fig. 1 where some absorption densities  $W = \rho |\Psi|^2 R^2$  are plotted. There are two special atomic states singled out in the capture process. One is the so called "upper" level which usually is the last that can be detected before the cascading down  $\bar{p}$  is absorbed. One can learn the width of this upper state measuring the intensity loss of the X-ray transitions. In  $^{58}\text{Ni}$ , and in many other nuclei, the nuclear absorption is most likely to happen from this level. The next circular state below is called the "lower" one. Sometimes, one can measure the shape of the X-ray lines feeding this lower state. Such measurements are possible when the lower state width is in the range of a few keV and additionally the rate of radiation from the upper state competes successfully with the upper state absorption rate. Chances for antiprotons to reach the "upper" levels have not been measured. Presumably a significant fraction of the antiprotons is absorbed in states of much higher principal quantum number  $n$ . Such a conclusion is reached in the kaonic atoms where the X-ray transition intensities for the lower atomic per stopped kaon are known to be about 0.2 to 0.6, [6]. For the studies of  $n/p$  ratios however the value of  $n$  is not very important, one needs to know mainly the distribution of capture states in terms of the angular momentum  $l$ , as at nuclear distances all atomic wave functions of the same  $l$  differ only by irrelevant normalisations. Calculations, [37], indicate the dominance of  $l = l_{\text{upper}}$  states in

the nuclear capture process. We discuss the uncertainties in this respect in the last section, here we calculate the absorption probabilities assuming full occupation of the  $l = l_{\text{upper}} + 1$  circular level. The capture probabilities from several circular states are given in Table I. The lower widths are usually larger than upper widths by two orders of magnitude. That is due to the smaller orbit radii and reduced centrifugal barriers. However, the absorption density profile is not changed dramatically as may be seen from the ratio of these densities given in Fig. 1.

The  $^{58}\text{Ni}$  nucleus is our reference case. Amongst the nuclei tested by the recent  $\bar{p}$  capture experiment, [1] see Table II, it is the simplest to describe.

The localisation of nuclear capture depends on the range of  $N\bar{N}$  forces. One way to find this range is to use  $N\bar{N}$  potential models, another perhaps more advantageous, is to fit the atomic and low energy scattering data. An early choice was to use charge density profiles for the  $\rho$ , [8,9,11]. This is equivalent to folding a form-factor  $v(\mathbf{u})$  in Eq.(2) of 0.8 fm rms range. More recently, longer ranged gaussian profile formfactors  $\exp(-(r/r_0)^2)$  have been used, [12,13]. Typical best fit values are:  $r_{0i} \approx 1$  fm (for  $\text{Im}V$ ) and  $r_{0r} \approx 1.5$  fm (for  $\text{Re}V$ ). On the other hand, calculations based on the  $N\bar{N}$  potentials yield average ranges  $r_{0i}$  of 0.75 fm up to 1.45 fm, [18,23], the difference being due to different handling of the off-shell extensions. An effect of the range is shown in Fig. 1. A longer  $N\bar{N}$  absorption radius broadens the region of nuclear absorption. The related effect on the  $n/p$  ratio measurement is shown in Fig. 2 and discussed later.

Optical model calculations based on the  $N\bar{N}$  interaction potentials [18–21] indicate that the lengths  $t_{N\bar{N}}$  bear no simple relation to the  $N\bar{N}$  S-wave scattering lengths which are smaller and repulsive i.e. with real parts positive. Thus,  $\text{Re}t_{N\bar{N}}$  is of a complicated and uncertain structure. At the extreme nuclear surface it reflects a long attractive tail of the pion exchange forces, about the nuclear radius it may turn to repulsion due to repulsive scattering lengths, and is rather uncertain at the nuclear matter densities. On the other hand, the phenomenological best fit  $\text{Im}t_{N\bar{N}}$  represents cumulative effect of the S and P wave absorptive amplitudes, and can be well understood in terms of the free  $\text{Im}t_{N\bar{N}}$ . The calculated optical potentials indicate structure more complicated than that given by formula (1), but cannot reproduce the data as accurately as the latter with the best fit parameters. In this calculation we use the phenomenological approach.

The level widths discussed so far reflect all modes of the nuclear absorption of antiprotons. The initial stage, an elementary  $N\bar{N}$  annihilation, generates an energy of 2 GeV of which 3/4 is the kinetic energy taken by the final state mesons. The mesons may excite the residual nucleus via inelastic scattering and absorption. To calculate the total widths one sums over the unobserved nuclear excited states. The large energy release and peripherality allows to use closure over the nuclear states. As a consequence the effective  $\text{Im}t_{N\bar{N}}$  is close to the absorptive part of free  $N\bar{N}$  scattering amplitude. That is

no longer true when the final nuclear states are limited to some particular states, as is the case of radiochemical methods that detect "cold" nuclei. The experiments in question, [1], allow only final nuclei excited up to the neutron separation threshold. Residual nuclei of higher excitations would decay by a neutron emission and would not be detected by the radiochemistry. In the next subsections the spectrum of allowed excited states is related to the rearrangement - and to interactions of final state mesons.

Now, to explain our aim we give a simplified result, which will be proven and refined later. Let  $s$  denote quantum numbers of the annihilated nucleon (neutron or proton), the antiproton atomic orbital  $(n, l, j)$  and the final state of the residual nucleus (any nucleus or cold nucleus). We are going to prove a simple expression for the partial absorption width  $\Gamma_s$  corresponding to the "cold" nucleus formation. In the zero force range limit this reads

$$\Gamma_s = 4 \frac{\pi}{\mu_{N\bar{N}}} \text{Im} t_{N\bar{N}}^s \int d\mathbf{R} |\Psi_{\bar{N}}(\mathbf{R})|^2 \rho_s(\mathbf{R}) P_s(\mathbf{R}) \quad (4)$$

In this expression a function  $P_s$  is introduced to describe formation of the required final states. It is a product of two terms  $P_s = P_{\text{miss}} * P_{\text{dh}}$ . The dominant factor in  $P_s$  is  $P_{\text{miss}}$  - the probability that the mesons born at point  $\mathbf{R}$  do not excite the residual nucleus, (missing probability of Ref. [1]). The other final state factor -  $P_{\text{dh}}$  is related to the final nucleus rearrangement and happens to be less significant. Examples of these functions are given in Fig. 2. The integrand in Eq.(4), including the  $R^2$  factor, is the absorption density for those processes that lead to the cold  $(A - 1)$  residual nuclei. It is shown as  $A$  in Fig. 2, in comparison to the full absorption density  $W$  given in Fig. 1 it is shifted to the periphery by almost 1 fm.

Now, we derive Eq.(4), calculate  $P_{\text{miss}}$ ,  $P_s$  and study the range effects.

### A. Nuclear $N\bar{N}$ annihilation and final state interactions

The aim of this section is to calculate the rate of nuclear  $\bar{N}$  annihilations that lead to cold final nuclei. This is done in several steps:

1) An amplitude for the  $N\bar{N}$  annihilation into mesons  $t_{N\bar{N} \rightarrow M}$  is assumed and introduced into the nuclear transition amplitude in the impulse approximation.

2) The emission probabilities are calculated and summed over the mesonic and nuclear final states. For an isolated  $N\bar{N}$  annihilation this procedure would produce the absorptive cross section and, via the unitarity condition, the absorptive amplitude  $\text{Im} t_{N\bar{N}}$ . For nuclear captures leading to cold nuclei we limit the summation over final states to the states of elastic meson-nucleus scattering. This limited summation generates the  $\text{Im} t_{N\bar{N}}$  again, but now it is folded over nuclear final state interaction factors.

3) To simplify our considerations, effects related to finite range of the reaction: propagation of the final mesonic resonances, recoil effects, nonlocalities due to external fields and the size of mesonic source are discussed at the end of this section.

Assume, that an antiproton in an  $n$ -th atomic state annihilates on a nucleon in a single particle state  $\alpha$  into  $k$  mesons with momenta  $p_i$ ,  $i = 1$  to  $k$ . In the impulse approximation, the transition amplitude for this process, is

$$A_{n,\alpha} = \int \Psi_{\bar{N}}^n(\mathbf{x}) \varphi_N^\alpha(\mathbf{y}) t_{N\bar{N} \rightarrow M}(\mathbf{x}, \mathbf{y}, \xi) \prod_i \bar{\varphi}_M(\mathbf{p}_i, \xi_i, \beta) \quad (5)$$

where  $\Psi_N(\mathbf{x})$  is the atomic,  $\varphi_N(\mathbf{y})$  the nuclear, and  $\varphi_M$  the mesonic wave function. The latter describes scattering states and corresponds to the ingoing boundary condition. The final state of the nucleus is not specified, in the spirit of the impulse approximation it is the initial nucleus that is left with a hole in the single particle state  $\alpha$ . Additional nuclear excitations follow nonelastic interactions of the mesons. States generated in this way are denoted by index  $\beta$  in the mesonic wave functions.

The transition amplitude  $t_{N\bar{N} \rightarrow M}(\mathbf{x}, \mathbf{y}, \xi)$  is not known in detail. What one needs for atomic studies is, basically, the elastic  $\text{Im}t_{N\bar{N}}^s$  extended off-shell. The momentum extension is related to the range dependence expressed in terms of the  $N\bar{N}$  relative coordinate  $\mathbf{x}-\mathbf{y}$ . As already discussed this is fairly well known, contrary to the range dependence in the mesonic coordinates  $\xi$ . The kinematic conditions are special since both the  $N$  and  $\bar{N}$  are bound and the pair energies fall below the  $N\bar{N}$  threshold. Even at these energies, the nuclear momenta reach  $1-2 \text{ fm}^{-1}$  and the scattering matrix should include at least S and P waves with all possible spin states. The relevant partial cross sections or partial absorptive amplitudes  $\text{Im}t_{N\bar{N}}$  could be calculated from potential models of the  $N\bar{N}$  scattering. Such a procedure is adopted in some optical potential calculations, [18–22], even-though the partial wave analysis of the  $N\bar{N}$  scattering does not exist. Unfortunately, the problem discussed here is more involved and uncertainties are larger. We aim, rather, at a semi-phenomenological "effective  $\text{Im}t_{N\bar{N}}^s$ " as used in the phenomenological optical potential.

To calculate the absorption widths, the amplitudes (5) are mod-squared, summed over the final pionic channels and integrated over the phase space. One has to sum also over the final nuclear states. In this way one arrives at an expression for the partial absorption widths  $\Gamma_s$

$$\Gamma_s = 4 \frac{\pi}{\mu_{N\bar{N}}} \int \Psi_{\bar{N}}(\mathbf{x}) \varphi_N^\alpha(\mathbf{y}) I^s(\mathbf{x}, \mathbf{y}, \mathbf{x}', \mathbf{y}') \bar{\Psi}_{\bar{N}}(\mathbf{x}') \bar{\varphi}_N^\alpha(\mathbf{y}') \quad (6)$$

where

$$I^s = \sum_{\beta} \sum_k \int dL \int d\xi \int d\xi' t_{N\bar{N} \rightarrow M}^s(\mathbf{x}, \mathbf{y}, \xi) \varphi_M(\mathbf{p}, \xi, \beta) \bar{\varphi}_M(\mathbf{p}, \xi', \beta) \bar{t}_{N\bar{N} \rightarrow M}^s(\xi', \mathbf{x}', \mathbf{y}') \quad (7)$$

Here, the integration  $dL$  means pionic Lorentz invariant phase space restricted by the energy conservation and  $k$  is the pion multiplicity. For an isolated  $N\bar{N}$  system at or below the threshold,  $I^s$  in Eq.(7) is related by the unitarity to absorptive part of the elastic  $N\bar{N}$  scattering amplitude

$$I^s = \text{Im}t_{N\bar{N}}^s(\mathbf{x} - \mathbf{y}, \mathbf{x}' - \mathbf{y}') \delta(\mathbf{R} - \mathbf{R}') \quad (8)$$

where  $\mathbf{R} = (\mathbf{x} + \mathbf{y})/2$  is the  $N\bar{N}$  CM coordinate.

For an annihilation inside a nucleus this free space unitarity relation is no longer true. In the external nuclear field the propagation of intermediate particles in Eq.(7) changes. If one is interested in the total annihilation rates the summation extends over the mesonic as well as over all the nuclear states. In such a case the closure approximation applies to nuclear states. It is justified by the large energy release, peripherality of capture and short annihilation range. Detailed calculations, [18–22], have been done for  $\bar{N}$  optical potentials with models that simulate mesonic channels by complex  $N\bar{N}$  potentials. These indicate difficulties of this question at nuclear matter densities. The effects of the external nuclear field become noticeable already at  $\rho = 0.1\rho(0)$  but reflect mainly on the  $\text{Re}V^{\text{opt}}$ . The antiprotonic atom physics discussed here is located safely below this density limit. This qualitative picture justifies the success of optical potential calculations that can relate the overall antiproton absorption rates to the free values of  $\text{Im}t_{N\bar{N}}$ . On the other hand, to describe the experimental results corresponding to the measurements of Ref. [1] one limits the sum in Eq.(7) to cold final nuclei. First we discuss the chance that the mesons created in the annihilation would leave the residual nucleus in such states of low excitations. Another excitation mode, the rearrangement is discussed afterwards.

The spectrum of mesons consists essentially of pions correlated in a sizable fraction into  $\rho$  and  $\omega$  resonances. These heavy mesons are very broad and after some 1 fm propagation range turn to the pions. Their multiplicities range from 2 to 8 with an average 4–5 and the average momentum is as large as  $2 \text{ fm}^{-1}$ . Nuclear interactions of these pions may be absorptive, inelastic or elastic. Those involving a pion absorption occur on two or more nucleons and produce  $(A - 2)$  or lighter nuclei. The inelastic processes end up with excited nuclei. These may be the  $(A - 1)$  nuclei of interest as the dominant mechanisms involve single nucleon excitation modes:  $\Delta$  and higher resonances. For medium and heavy nuclei, and pionic energies around  $\Delta$  the inelastic cross sections reach 0.5 b [30]. The main strengths are located much higher than neutron emission thresholds, however. Cross sections for excitations of states below these limits are typically 1-10 mb, [31]. On the other hand the elastic cross sections are

very large and reach 1 b, [30]. Hence, the rate for production of cold nuclei is given essentially by the elastically scattered waves. This allows an optical potential description. In addition, in the bulk of phase space the pions are fast enough to allow an eikonal description. Following this the wave function for each pion is taken in the form

$$\bar{\varphi}_M^{(-)}(\mathbf{p}\xi) = \exp(i\mathbf{p}\xi - iS(\mathbf{p}, \xi)) \quad (9)$$

with  $S$  calculated in terms of the pion-nucleus optical potential

$$S(\mathbf{p}, \xi) = \int_0^\infty ds \left( \sqrt{(p^2 - U^{\text{opt}}(\xi + \frac{\mathbf{P}}{p}s) - p)} \right) \quad (10)$$

The function  $S$  is calculated in a quasi-classical way by integrating the local momentum over the straight line trajectory. Due to nuclear excitations and pion absorptions this wave is damped with a rate described by  $\text{Im}S$ . The latter is generated by absorptive part of the pionic optical potential  $\text{Im}U^{\text{opt}}$ . This damping follows the whole path of a pion but the main effect comes from regions of large nuclear densities and not the region around the birth place  $\xi$ . We assume that all functions  $S(\mathbf{p}, \xi)$  are related to the central point of annihilation  $\mathbf{R}$  which is the  $N\bar{N}$  CM coordinate. Effects of the source size are discussed later, jointly with consequences of the heavy mesons propagation range. The assumption on the emission of mesons from the central point substantially simplifies our calculations. With the mesonic wave functions (9) which enter Eq.(7), the total momentum of mesons  $\mathbf{P}$  separates to a plane wave form. Some additional dependence on  $\mathbf{P}$  is still there but as we show later it is rather weak. One consequence is that the  $N\bar{N}$  CM "conservation"  $\delta(\mathbf{R} - \mathbf{R}')$  which arises in the free unitarity relation (8) is also a good approximation in the nuclear case (7). Now the final state pion interaction factors that enter Eq.(7) may be collected into a function

$$P^k(\mathbf{R}) = \langle \prod_i |\exp(-S(\mathbf{p}_i, \mathbf{R}))|^2 \rangle \quad (11)$$

which is a product of the eikonal factors within each multiplicity  $k$ . It has to be averaged over the multiplicities and the pionic phase space weighted by some unknown momentum dependence generated by  $t_{N\bar{N}\rightarrow M}$ . The expectation is that the momentum dependence of  $P^k$  is weak as compared to the momentum dependence of  $t_{N\bar{N}\rightarrow M}$  since the former is determined by the nuclear size and the latter by the size of annihilation region. Thus one may expect the unitarity condition to hold approximately provided the averages of  $P^k$  in Eq.(7) are factored out. This averaging is now performed and in this way one arrives at

$$I^s \approx \text{Im}t_{N\bar{N}}^s(\mathbf{x} - \mathbf{y}, \mathbf{x}' - \mathbf{y}')\delta(\mathbf{R} - \mathbf{R}')P_{\text{miss}}(\mathbf{R}) \quad (12)$$

where the "missing probability" is given by

$$P_{\text{miss}}(\mathbf{R}) = \sum_k w_k \int dL f(p_i) \prod_k |\exp(-S(\mathbf{p}_i, \mathbf{R}))|^2 / \sum_k w_k \int dL f(p_i) \quad (13)$$

The integration extends over the restricted Lorentz phase space weighted by an experimental multiplicity distribution  $w_k$ , for  $k$  from 2 to 8, [15,16]. In order to check the assumptions, some factors  $f(p_i)$  have been introduced into Eq.(13), while pure phase space and constant  $t$  matrices correspond to  $f = 1$ . This probability density selects those pionic interactions that do not excite the residual nucleus.

Calculations of  $P_{\text{miss}}$  are performed in a Monte Carlo procedure. The optical potential for pions must cover a wide momentum range from the threshold up to 0.9 GeV but the phase space favours a region just above the  $\Delta$  resonance. This potential is related to the pion nucleon forward scattering amplitudes and in this way to the pion nucleon cross sections. That method is well established around the  $\Delta$ , [27]. Here, this procedure is extended to cover also higher  $N_{11}^*$ ,  $N_{13}^*$  resonances which are described by Breit-Wigner amplitudes. The two nucleon absorption mode is taken in a phenomenological form [28]. Performing these calculations one finds that: high energy expansion of the square root in Eq.(10) is satisfactory, higher resonances cannot be neglected and the black sphere limit is a good approximation in dense regions. In particular  $P_{\text{miss}}(\mathbf{R})$  is changed by less than 10 percent with an inclusion of the two nucleon absorption. The latter being of the  $\rho^2$  profile operates in the region where the black sphere limit is well fulfilled. An example of calculated  $P_{\text{miss}}(\mathbf{R})$ , given in Fig. 2, is close to a pure geometrical estimate that relates it to the solid angle of the nucleus viewed from the point  $\mathbf{R}$ , [15]. Nevertheless, the gray zone at the nuclear surface make the effective radius of an equivalent black sphere difficult to predict off-hand.

The  $P_{\text{miss}}(\mathbf{R})$  calculated in this way is at best semi-quantitative, but the proximity of strong absorption limit makes the result fairly independent on the details of the annihilation. One question is that the phase space alone does not reproduce the experimental momentum distribution of a single pion, [17]. To remove the discrepancy some factors  $f(p_i)$ , which generate the correct distribution, have been introduced into average (13). Now, corrected in this way  $P_{\text{miss}}(\mathbf{R})$  is shown in Fig. 2, it is seen to differ only slightly from the pure phase space result. As the corrective procedure is uncertain and the change is below experimental uncertainties we follow the pure phase space averaging.

In the surface region of interest, the missing probabilities  $P_{\text{miss}}$  rise linearly with the distance  $R$ . That is a fortunate result, it makes  $P_{\text{miss}}$  rather insensitive to the size and structure of the annihilation region located in a small sphere around  $\mathbf{R}$ . The same applies to effects of the  $\rho$  and  $\omega$  mesons. These may propagate some distance to a point  $\mathbf{R}'$  and decay into pions there. Those events

are approximately confined to within a sphere centered at  $\mathbf{R}$  of a radius = velocity \* lifetime  $\approx 1$  fm. Again, the linearity of  $P_{\text{miss}}(\mathbf{R}')$  makes an averaged pionic missing probability equal to the  $P_{\text{miss}}(\mathbf{R})$ .

Let us turn now to other corrections. The annihilation happens at the nuclear surface and is confined to a region of a small diameter. Nevertheless, effects of the nucleus should be considered. These are: the  $N\bar{N}$  centre of mass motion, external field, and Pauli principle in the intermediate states. At distant surface most of these have been found small in the optical model calculations. Now we discuss briefly the implications in the  $A-1$  reactions. The first, elementary effect due to the presence of nucleus is the  $N\bar{N}$  centre of mass motion with respect to the residual nucleus. It is given by the recoil energy i.e. by a Fourier transform of  $t_{N\bar{N}}(E - P^2/4M)$  over the  $N\bar{N}$  CM momentum  $P$ . It is known in the kaonic atoms [4,5] that a narrow (30 MeV or less) resonance close to the threshold would induce a propagation range as large as 1 fm and affect strongly the peripherality of nuclear capture. Extensive experimental efforts gave no clear evidence for narrow resonances in the  $N\bar{N}$  system close to the threshold. Energy independent transition matrices  $t_{N\bar{N} \rightarrow M}$  are assumed here. Hence the annihilation is fast and the  $N\bar{N}$  CM may be fixed in the absorption process, thus a factor  $\delta(\mathbf{R} - \mathbf{R}')$  is justified in Eq.(12). On the other hand, an effect of the CM motion arises due to dependence of the pionic functions  $S(\mathbf{p}_i, \mathbf{R})$  on the total momentum of mesons  $\mathbf{P}$ . It induces some nonlocality in the  $\mathbf{R} - \mathbf{R}'$  but the effect enters in a second order of a small quantity  $P/(\text{pion momentum})$ . Numerical studies described earlier indicate a nonlocality of a 0.1 fm range, negligible in comparison to the 1 fm range effects involved in the relative coordinate  $\mathbf{x} - \mathbf{y}$ .

## B. Range effects

In the limit of zero range  $N\bar{N}$  interactions formula (6) for the partial absorption width may be expressed in terms of nuclear densities. For finite-ranged interactions the single particle wave functions involved may be reduced only to mixed densities. However, for simplicity and historic reasons one wants to have an approximate expression in terms of the true densities. At the nuclear surface this can be done with a good precision, at least for the absorption rates summed over all nucleon states. The standard relation, [24], that allows it is:

$$\sum_{\alpha} \bar{\varphi}_i^{\alpha}(\mathbf{y}') \varphi_i^{\alpha}(\mathbf{y}) \approx \rho_i(\mathbf{Y}) j_0(k_F(\mathbf{Y}) |\mathbf{y} - \mathbf{y}'|) \quad (14)$$

where  $\mathbf{Y} = (\mathbf{y} + \mathbf{y}')/2$ ,  $k_F$  is an effective local Fermi momentum which may be calculated in a shell model and  $i = p, n$ . In a similar way we express the angular averaged atomic wave functions  $\bar{\Psi}\Psi$  by

$$\frac{1}{2l+1} \sum_m \bar{\Psi}_{N\bar{N}}^n(\mathbf{x}') \Psi_{N\bar{N}}^n(\mathbf{x}) \approx |\Psi_{N\bar{N}}^n(\mathbf{X})|^2 \{D^n(\mathbf{X} - \mathbf{X}') + O(\mathbf{X}/nB, \mathbf{X}'/nB)\} \quad (15)$$

It is an expansion in the inverse Bohr radius of the orbit  $1/nB$  and calculation of function  $W$  is straightforward.

Finally, to handle the  $N\bar{N}$  ranges we assume a separable approximation for the scattering matrix in Eq.(12)  $t_{N\bar{N}} = v(\mathbf{x} - \mathbf{y}, r_0\sqrt{2}) t_{N\bar{N}}^0 v(\mathbf{x}' - \mathbf{y}', r_0\sqrt{2})$  and gaussian form-factors  $v$  with some range parameters  $r_0$ . This allows for a simple transformation to relative coordinates and reduces Eq.(6) into a folded density expression, [18]. For the capture rates one has now:

$$\Gamma_s = 4 \frac{\pi}{\mu_{N\bar{N}}} \text{Im} t_{N\bar{N}}^0 \int |\Psi_{N\bar{N}}(\mathbf{Y})|^2 v(\mathbf{Y} - \mathbf{X}, r_0) f_X \rho_i(\mathbf{X}) P_{\text{miss}}^s\left(\frac{\mathbf{X} + \mathbf{Y}}{2}\right) \quad (16)$$

where  $f_X$  is a factor that collects together a large piece of finite range effects

$$f_X = \int d\mathbf{u} v(\mathbf{u}, 2r_0) j_0(k_F(\mathbf{X})\mathbf{u}) D(\mathbf{u}) \quad (17)$$

With a normalised form-factor  $v$  the limit of zero range force is  $f_X = 1$ . For a typical  $N\bar{N}$  absorption range  $r_0 = 1$  fm values of  $f_X \sim 0.5-0.6$  are obtained. These are almost constant in the nuclear surface region of interest and may be taken out of the integral. As our analysis involves only ratios of the widths the actual values of  $f_X$  are unimportant.

The summation in Eq.(14) selects capture events that lead to single hole nuclear states. These do not correspond to the experimental conditions that require cold final nuclei or, more precisely, nuclei either in the ground states or in states excited below the neutron emission threshold  $T_n$ . To account for it we limit the sum over the initial nucleon states in Eq.(10) to those that leave the final nucleus with excitation energies less than  $T_n + 2$  MeV where the 2 MeV is allowed for neutron kinetic energies. At the surface almost all single particle states of sizable overlap with the atomic antiprotons contribute to the sum. The experimental cut-off that eliminates deeply bound nucleons becomes a (small) correction, which we call a "deep hole" factor. Defined as the ratio of limited sum of single nucleon densities to the total sum  $P_{\text{dh}}(\mathbf{X}) = \sum_{\alpha}^{\text{ld}} \varphi_{\alpha}^2 / \sum_{\alpha} \varphi_{\alpha}^2$  and implemented into the partial width formula produces

$$\Gamma_s(\text{cold}) = 4 \frac{\pi}{\mu_{N\bar{N}}} \text{Im} t_{N\bar{N}}^0 f_X \int |\Psi_{N\bar{N}}(\mathbf{Y})|^2 v(\mathbf{Y} - \mathbf{X}, r_0) \rho_i(\mathbf{X}) P_{\text{dh}}(\mathbf{X}) P_{\text{miss}}\left(\frac{\mathbf{X} + \mathbf{Y}}{2}\right) \quad (18)$$

This is our result and now we turn to practical, model calculations of the basic ingredients in this equation.

### III. CALCULATIONS OF NUCLEAR DENSITIES

For the first test we use an asymptotic density (AD) model. It follows, essentially, the Bethe-Siemens approach [25] but it also incorporates larger phenomenological input i.e. charge density distribution, neutron and proton separation energies and difference of the rms radii of proton and neutron densities. At central densities a Fermi gas of independent protons and neutrons is assumed. The Fermi momenta are determined by the densities and the Fermi energies are fixed by the separation energies. This gives the depth of the potential well which in the surface region is extrapolated by the Woods-Saxon form. The densities are given by the exponential damping of the nucleon wave functions due to the potential barriers. For protons a Coulomb barrier is added and potential parameters (half-density radius  $c$  and the surface thickness  $t$ ) are fitted to reproduce the experimental charge density down to 5 percent of the central density. For neutrons the same  $t$  is used but  $c$  is chosen to obtain the rms radius equal (or larger by 0.05-0.10 fm in the heaviest nuclei, [36]) to the proton density rms radius. This model is expected to generate average level densities, it misses shell effects and correlations.

As a second method to determine neutron and proton densities we have used a selfconsistent Hartree-Fock theory with the effective two-body Skyrme-type interaction. Since our aim in using HF method was rather unusual, i.e. to find nucleon densities at the extreme tails of the nuclear matter distribution (at distances of 8–15 fm from the center), a few remarks about its practical implementation seem to be in order here.

The necessary practical condition is the use of a HF code not restricting in any way the asymptotic form of s.p. wave functions. This condition excludes e.g. all codes using the harmonic oscillator basis. In the present work we have applied the code solving HF equations on the spatial mesh, in which all fields and densities are expressed in the coordinate representation.

The most severe restriction of the presented results is the imposed spherical symmetry. It allows enormous simplification of solution, in particular the HF equation takes the form of a differential equation in the radial variable for each pair of the conserved s.p. quantum numbers  $l$  and  $j$ . We used 100 mesh points in the radial coordinate, in a box of the size of 25 fm and put as a boundary condition the values of the wave functions at the far end of the box equal to zero.

The density matrix is obtained by summing contributions from the lowest s.p. orbits. If necessary, the contribution of the last orbit is calculated in the filling approximation; i.e. an appropriate occupation probability, smaller than one, is associated with this orbit.

The asymptotic form of the radial s.p. wave function for large  $r$  corresponding to the s.p. energy eigenvalue  $\epsilon_{nlj}$  is

$$\mathcal{R}_{nlj}(r) = w_l \left(\frac{1}{r}\right) \exp(-\kappa r)/r, \quad (19)$$

where  $\kappa = \sqrt{\frac{2m}{\hbar^2} |\epsilon_{nlj}|}$  and  $w_l$  is a polynomial with the dominant term being a constant, so that the contribution to the asymptotic density is proportional to  $\exp(-2\kappa r)/r^2$ . For proton orbitals there is an additional exponential factor, coming from the Coulomb barrier and modifying  $\kappa_p$ , which is very important for distances in question, i.e., between 7 and 15 fm. Although at very large distances from the center the neutron to proton density ratio is proportional to  $\exp(2(\kappa_p - \kappa_n)r)$ , where  $\kappa_n$  and  $\kappa_p$  are directly related to neutron and proton separation energies, respectively, at distances near the  $\bar{p}$  absorption peak usually a few neutron and proton orbitals contribute significantly to the density and a more detailed analysis is necessary to evaluate the latter.

S.p. binding energies (Fermi levels) important in determination of nuclear density tails are not reproduced exactly with existing effective Skyrme forces. In addition, calculated spherically symmetric densities for deformed nuclei lack quadrupole correlations which *a priori* may for their own sake distort positions of the Fermi levels. Therefore, calculated densities, especially for deformed nuclei, must be treated as approximate, and possible sources of error must be kept in mind. In particular, the true densities of deformed nuclei may have longer tails since their elongated form has to be smeared over Euler angles in order to obtain spherically symmetric density in the LAB frame.

In spite of the approximate character of our nuclear density calculations we used also HFB theory [33,34] in order to assess modifications introduced to HF results by the residual pairing interaction. In the present case it must be distinguished from the very often used HF+BCS method, in which the pairing correlations are included using the BCS prescription to self-consistent orbitals. In the latter case, the partial occupation of orbitals above the Fermi level leads to a non-zero, though usually minuscule, occupation of orbitals of positive energy (in continuum). Since such orbitals are not localized this implies that they dominate nuclear density at large distances which is a completely unphysical effect.

The applied HFB code also uses the coordinate representation and the HFB equations are solved on a spatial mesh. The proper analysis of the asymptotic properties of two-component quasiparticle wave functions shows [35] that the HFB ground state wave function, even containing pairing correlations, is always localized if bound. The asymptotic form of the occupied negative-energy quasiparticle states is as in the Eq.(19), with  $\kappa$  defined in terms of the sum  $E_{nlj} - \lambda$ , where  $E_{nlj}$  is the quasiparticle energy and  $\lambda$  is the Fermi energy.

As the effective force we use the ten-parameter Skyrme SkP interaction described in Ref. [35]. It has a virtue that the pairing matrix elements are determined by the force itself, contrary to other Skyrme-type interactions which define only the particle-hole channel. In the paired HFB

ground-state the pairing gap is state dependent. As a simple pairing gap parameter one can use the pairing potential average over the occupied states.

The "deep hole" corrective factor in the HFB method is calculated using the additional condition in the form  $\epsilon_n < \lambda$ , where  $\epsilon_n$  are the expectation values of the self-consistent mean-field matrix (not q.p. energies) and  $\lambda$  is the HFB Fermi energy.

The last method we used for determination of nuclear densities was chosen to assure correct separation energies. A single particle (SP) spherical well, including the central and spin-orbit potentials for neutrons and protons was assumed. Proper order of s.p. levels is guaranteed by the form of the potential. Potential parameters were adjusted slightly to obtain the experimental separation energies, charge rms radii and, if known, the neutron rms radii.

## IV. RESULTS

In this section we discuss the partial antiproton absorption widths:  $\Gamma_n(A-1)$  and  $\Gamma_p(A-1)$  for captures on a neutron and proton, respectively, which produce cold  $(A-1)$  final nuclei. Sum of the two is denoted by  $\Gamma(A-1)$ . Experiments determine those partial widths relative to the total absorption width  $\Gamma^{\text{tot}}$ . The data collected in Table II consist of two such ratios:  $\sigma_{A-1} = \Gamma(A-1)/\Gamma^{\text{tot}}$  and  $\sigma_{np} = \Gamma_n(A-1)/\Gamma_p(A-1)$ . The first one  $\sigma_{A-1}$  is a test for a description of the antiproton absorption. In particular it checks the weakest points: understanding of the final state interactions and knowledge of the initial atomic states of capture. If quantitative understanding is achieved one can claim control over the region of nuclear surface where the neutron halo is measured. The halo itself is seen via the  $\sigma_{np}$  ratio.

### A. The $\sigma_{A-1}$ ratios

A typical antiproton absorption scenario is visualized in Fig. 1 and Fig. 2, which contain some ingredients of formula (18) for the capture widths. The results, given in Table I, show  $\sigma_{A-1}$  calculated for some circular atomic orbits that are most likely to be the states of nuclear capture. The shapes of  $(A-1)$  capture densities are determined by the angular momentum  $l$ , strong nuclear absorption and  $P_{\text{miss}}$  and thus are rather independent on the normalisation of the atomic wave functions i.e. on  $n$ . Thus, these ratios are typical to all  $n$  states. With the angular momentum  $l$  increased by one unit, in particular from the "lower" to the "upper" and higher  $l$  states, the  $\sigma_{A-1}$  increases by about 20%. Thus, the experimental data exclude sizable fraction of high  $l$  captures but seem less restrictive on the states with  $l$  lower than  $l_{\text{lower}}$ , where the calculated  $\sigma_{A-1}$  stabilises. On the other hand,

cascade calculations done in kaonic, hyperonic and antiprotonic atoms, [6,37], show the nuclear capture from the latter very low  $l$  states to be unlikely. Also, these calculations indicate an accumulation of the capture probability on two or at most three values of  $l$ . This result is consistent with our capture probabilities, given in Table I, and calculated under the extreme assumption that the  $l = l_{\text{upper}} + 1$  circular level is fully occupied at some stage of the atomic cascade. On the other hand, calculations of Ref. [7] allow a broader distribution with a 20 percent share of the  $l_{\text{upper}} + 1$  and higher  $l$  states and a 10 percent share of  $l_{\text{lower}} - 1$  values. If that is the real situation our results for  $\sigma_{A-1}$  and  $\sigma_{np}$  would rise typically by a factor of 1.05. This is the likely uncertainty of the calculations in Tables I, II due to poor knowledge of the capture orbits. One hopes to clarify some of these points by experimental measurements of the cascade intensities and absolute cascade intensities in the nuclei of interest, [14].

The  $\sigma_{A-1}$  calculated with the AD and other models are consistent with most of the experimental data, shown in Table II. This gives some confidence in the validity of the final and initial state description. However, there are two outstanding discrepancies: Te and Yb.

*Special cases of  $^{130}\text{Te}$  and  $^{176}\text{Yb}$*

The first case is understood qualitatively, the second presents a point of specific interest. It is known experimentally [26] that a strong E2 mixing, i.e. coupling of the atomic and nuclear rotations, occurs in the upper level of the  $^{130}\text{Te}$  atom. It stimulates absorption from the upper level as indicated in Table I, and induces an effect of alignments of the nuclear and atomic spins in the states admixed to the upper level. Thus the orbital antiproton stays closer to the elongated part of the nucleus, as compared to states of equally averaged orientations. Thus, the final pions have a better chance to miss the nucleus. Calculations yield some 20% enhancement of the total absorption widths due to this effect [26]. One expects similar enhancement of the  $\sigma_{A-1}$  rate, it is also likely that the  $n/p$  ratio is higher at the poles of this nucleus. The strong E2 mixing happens also in  $^{176}\text{Yb}$  for high  $n = 14$  atomic orbits, however. It is not clear as yet what are the consequences for the atomic cascade process between the  $n = 14$  state and nuclear absorption. It is also not clear what correlation of the atomic motion and nuclear orientation is induced by this effect. Future experimental and theoretical studies [14] will help to elucidate this point.

Antiproton absorption in the heaviest elements,  $^{232}\text{Th}$  and  $^{238}\text{U}$ , is accompanied by a nuclear fission of the final  $(A - 1)$  nuclei which, in principle, may affect the  $\sigma_{A-1}$  rate. However, in such nuclei the radiative rates dominate the fission rates for excitations less than the neutron emission threshold, [38]. In the even-odd nuclei of interest this domination is even stronger. Thus, the fission channel is expected to change the  $\sigma_{A-1}$  only a little, and this is apparently borne out by the data in Table II.

## B. The $\sigma_{np}$ ratios

The partial absorption widths are proportional to effective absorptive amplitudes  $\text{Im}t_{N\bar{N}}$  for the  $\bar{p}n$  and  $\bar{p}p$  pairs. These are not well known, although some average values follow from the optical potential phenomenology. The number required for neutron halo studies is a ratio  $R_{np} = \text{Im}t(\bar{p}n)/\text{Im}t(\bar{p}p)$  which may be taken from other experiments. One value  $R_{np} = 0.63$  has been obtained by Bugg, [3], from measurements of charged pions emitted in the  $\bar{p}$  absorption in Carbon. Difficulties arise since it includes effects of final state mesonic interactions and the inherent uncertainties of the charge exchange reactions. This value of  $R_{np}$  generates mild disagreement with the data of Ref. [1] for all the nuclei and all nuclear models used here. The results given in Table I should be compared to the experimental data in Table II, similar discrepancies are generated by other models. A different result  $R_{np} = 0.81(3)$  follows from the stopped antiproton absorption in deuterium, [29]. This value is free from the pionic effects, but the deuteron kinematic conditions, in particular the binding energy, differ from those met at the nuclear surface. Another value of  $R_{np}$  obtained in  ${}^4\text{He}$  is smaller and energy dependent. At rest, a number  $R_{np} = 0.48(10)$  has been deduced from rather involved analyses of the final state mesonic interactions in the three nucleon systems [32].

In this work we fix  $R_{np}$  from a best fit to our simplest nucleus which is  ${}^{58}\text{Ni}$ . Our nuclear models yield similar results in this case and the fitted  $R_{np}$  is very close to the value obtained from the deuteron. We shall use the latter in our analysis.

The results for  $\sigma_{np}$  are collected in Table II. It is clear that the crudest model of asymptotic density strongly overestimates the  $\rho_n/\rho_p$  ratios at large distances. This property has been known already from the neutron pickup studies, [10]. By the same effect, the AD model produces too large  $\sigma_{A-1}$  in the heaviest nuclei Th and U. The physics behind it is quite transparent:

1) It is vital to have correct separation energies but these are not the whole story.

2) The Coulomb barriers enhance anomalously the  $\rho_n/\rho_p$  ratio at large distances. That has to be off-set by shell effects (angular momentum barriers) and correlations.

3) Proper setting of the neutron skin defined in terms of mean squared radii  $R_{ms}(\text{neutrons}) - R_{ms}(\text{protons})$  does not determine the "neutron halo". The latter are understood here in terms of  $\sigma_{np}$  i.e. ratios of high moments of density distributions.

What are the moments involved in the haloes measured by the radiochemical experiment? For zero range interactions and  $P_{\text{miss}} = 1$  these are the "Barret moments" i.e.  $2l$ -th moments due to centrifugal barriers corrected for the atomic wave functions. The  $P_{\text{miss}}$  and  $P_{\text{dh}}$  increase the order of the moments approximately by two units. On the other hand, the annihilation range effects,

i.e., the folding, introduces moments smaller by two, four and more units. The joint effect is best estimated by the dominant  $2l$  density moment involved. As we see from Table I these are very high moments ranging from 10 in Ni to 18 in U.

The HF method with the SkP force gives roughly correct neutron separation energies for (nearly) spherical systems  $^{58}\text{Ni}$ ,  $^{96}\text{Zr}$ ,  $^{144}\text{Sm}$ , underbinds the last neutron in  $^{96}\text{Ru}$  by 1.3 MeV but generally underestimates proton separation energies, e.g. by 1.1 MeV in  $^{144}\text{Sm}$  and by 3 MeV in  $^{58}\text{Ni}$ . This statement is qualitatively true also for the rest of deformed nuclei, with the one exception of  $^{154}\text{Sm}$  where the last neutron is underbound by 2.9 MeV. As we have checked in a separate calculation the Skyrme force SIII does not improve description of Fermi energies in the studied nuclei.

Comparison between the data and HF results shows clear disagreement for Yb and  $^{144}\text{Sm}$  and less pronounced one for Te, Th, and U nuclei. On the basis of comparison of calculated and experimental separation energies one can expect qualitatively corrections to the calculated  $\sigma_{A-1}$  and  $\sigma_{np}$  ratios (remembering that like errors in proton and neutron Fermi energies tend to compensate each other for the  $\sigma_{np}$ ). In all presented cases except  $^{144}\text{Sm}$  and  $^{176}\text{Yb}$  they go in the right direction.

In order to better understand the asymptotic HF densities one can look closer at how many orbitals contribute to it at large distances and to test by means of the formula (14) the sensitivity of the  $\rho_n/\rho_p$  ratio to shifts in s.p. energies. In  $^{58}\text{Ni}$ , at  $r = 7$  fm, two orbitals give about 35% of the neutron density each, 3 others give about 10% each. For protons, there is one orbital contributing 56% (the highest one) and three other contributing about 12% each. At  $r = 15$  fm, the last occupied orbitals contribute 89% and 91% to the neutron and proton densities, respectively. Of course, the heavier the nucleus, the farther the asymptotic region and the more orbitals contribute to one-body densities in the range 8-15 fm. In  $^{144}\text{Sm}$ , at  $r = 7$  fm, 4 states contribute more than 10% each to the neutron density (the highest percentage being 24%), four others contribute more than 5% each. Even at 15 fm, there are still 4 neutron orbitals contributing significantly to  $\rho_n$  (32%, 24%, 20% and 16%), the reason being that their s.p. energies differ not more than 4 MeV. In  $^{238}\text{U}$ , at 15 fm, one must account for 4 neutron orbitals while only two proton orbitals contribute 79% and 15% of the  $\rho_p$ . Clearly, it is not only a distance  $r$  but also the (sub)shell structure which decides how many orbitals contribute.

In order to estimate the effect of s.p. energies on the density ratio  $\rho_n/\rho_p$  we have used the following procedure. Contributions to the density at  $r = 8$  fm were used as a data and the propagation to  $r = 15$  fm was performed using Eq.(19), with account for the Coulomb barrier. The resulting densities for  $^{96}\text{Zr}$  are then larger than the exact HF densities roughly by the factor 7/4 and 9/7 for neutrons and protons, respectively. (The  $\rho_n/\rho_p$  ratio is then 161 instead of 115.) This error comes from the influence

of the polynomial  $w_l$  in Eq.(19) but we concentrate on the effect of changing s.p. energies on the so calculated  $\rho_n/\rho_p$  at  $r = 15$  fm. The decrease of the neutron energies by 1 MeV changes this ratio to 94, the decrease of the proton energies by 1 MeV rises the ratio to 234 and the simultaneous decrease of both proton and neutron energies by 1 MeV slightly decreases the ratio to 137. This gives some feeling as to the sensitivity of the  $\rho_n/\rho_p$  to the neutron and proton binding energies.

*Special case of  $^{58}\text{Ni}$*

This is our reference nucleus. The input data is certain and all model calculations produce consistent results. We use  $R_{ms}(n) = 3.734$  and  $R_{ms}(p) = 3.710$ , [36], which in the SP approach produce  $\sigma_{A-1} = 1.05$  and  $\sigma_{np} = 0.88$ . That is close to the HF and HFB results from Table II. The latter two methods are not perfect, HF underbinds protons by 0.5 and neutrons by 0.3 MeV. These errors are of no significance, however, since the absorption is spread over four neutron and four proton s.p. states.

*Special case of  $^{144}\text{Sm}$*

This nucleus displays a proton halo. Qualitatively, it might be due to the closed neutron shell. The separation energy of neutrons is large (10.6 MeV) with respect to a small (6.2 MeV) one for the protons. However, this proton halo effect is not reproduced in our calculations. Both results for  $\sigma_{np}$  given in Table II and plots of the *neutron/proton* density ratios given in Fig. 3 indicate a neutron excess at the surface. The separation energies in our nuclear models are either fitted to the experimental (AD or SP) or well reproduced for neutrons. For protons the HF model underestimates the experimental value by 0.9 MeV and that should even enhance the proton tail over the real one. This case indicates again that it is not only the separation energy that matters for the nuclear tail. The experimental result in  $^{144}\text{Sm}$  is not understood and opens the case for more exotic speculations.

One obvious effect of inclusion of pair correlations is a change in the  $\rho_n/\rho_p$  ratio in the tail of the density following from the change in the Fermi energy. At smaller distances however, this ratio may change in the opposite direction if other levels than the last one contribute to the density. It turns out that in all studied cases the change in the  $\rho_n/\rho_p$  due to pairing is small up to 14 fm. A much more pronounced pairing effect on both ratios  $\sigma_{np}$  and  $\sigma_{A-1}$  comes from the  $P_{dh}$  factor which e.g. in  $^{232}\text{Th}$  changes from 0.52 (no pairing) to 0.69 (with pairing) at the total absorption peak at  $r = 8$  fm. This change more than balances a decrease in  $\rho_n/\rho_p$  ratio providing for larger values of  $\sigma_{A-1} = 0.109$  and  $\sigma_{np} = 4.65$  (see Table II). The same  $P_{dh}$  factor is responsible for an increase of both ratios in  $^{238}\text{U}$ , to 0.100 and 4.31, respectively, while the smaller  $P_{dh}$  leads to smaller  $\sigma_{A-1}$  and  $\sigma_{np}$  in  $^{96}\text{Zr}$  (0.117 and 2.40, respectively). Pairing changes also  $\sigma_{A-1}$  for  $^{154}\text{Sm}$  to 0.106 and  $\sigma_{np}$  for  $^{154}\text{Sm}$  and  $^{176}\text{Yb}$  to 2.96 and 3.50, respectively. Changes due to pairing are nearly none for other nuclei.

## V. CONCLUSIONS

The radiochemical method which detects the products of nuclear capture of antiprotons is a valuable source of information on the relative *neutron/proton* density distribution on the extreme tail of nuclear surface. The main features which we want to stress are:

1) The nuclear regions tested are more peripheral than those studied by the X ray measurements in hadronic atoms. One measures essentially the  $2l$  moments of the density distributions where  $l$  is the angular momentum of "upper levels". These moments are as high as 18 in the heaviest nuclei.

2) There are special cases of alignment of nuclear and atomic angular momenta formed by the E2 mixing which display higher  $n/p$  ratios and higher rates of cold single nucleon captures. These may test the composition of the pole regions in deformed nuclei. Further studies are recommended.

3) The uncertainty in the initial atomic state of capture is kept under a fair control by the  $\sigma_{A-1}$  rates. However, additional X-ray experiments would be helpful to clarify this question.

4) Strong neutron haloes are observed in heavy deformed nuclei. These are not determined by the binding energies and Coulomb barriers alone. The shell effects (angular momentum) are also important. Few (two or three) of the highest nucleon orbitals contribute most to the cold capture rates.

5) An interesting case of a proton halo is found in  $^{144}\text{Sm}$ . It is not understood in terms of single particle models, and may signal strong nuclear correlations in the surface region.

6) Apart from the  $^{144}\text{Sm}$  case the nuclear models reproduce the qualitative features of the observed haloes.

We thank J. Jastrzębski for his constant interest and collaboration and P.E. Hodgson for his advice and for arranging the collaboration that was kindly supported by The Royal Society and KBN.

- 
- [1] J. Jastrzębski, H. Daniel, T. von Egidy, A. Grabowska, Y.S. Kim, W. Kurcewicz, P. Lubiński, G. Riepe, W. Schmid, A. Stolarz, and S. Wycech, Nucl. Phys. **A558**, 405c (1993); P. Lubiński, J. Jastrzębski, A. Grochulska, A. Stolarz, A. Trzcińska, W. Kurcewicz, F.J. Hartmann, W. Schmid, T. von Egidy, J. Skalski, R. Smolańczuk, S. Wycech, D. Hilscher, D. Polster, and H. Rossner, Phys. Rev. Lett. **73**, 3199 (1994).
  - [2] D.H. Wilkinson, Phil. Mag. **4**, 215 (1959); P.B. Jones, Phil. Mag. **3**, 33 (1958).
  - [3] W.M. Bugg, G.T. Condo, E.L. Hart, H.O. Cohn, and R.D. McCulloch, Phys. Rev. Lett. **31**, 475 (1973).

- [4] D.H. Davis, S.P. Lovell, M. Csejthey-Barth, J. Sacton, G. Schorochoff and M. O'Reilly, Nucl. Phys. **B1**, 434 (1967).
- [5] E.H.S. Burhop, Nucl. Phys. **B1**, 438 (1967); Nucl. Phys. **B44**, 445 (1972).
- [6] C.E. Wiegand and G.L. Godfrey, Phys. Rev. **A9**, 2284 (1974); R. Seki and C.E. Wiegand, Ann. Rev. Nucl. Sc. **25**, 241 (1975).
- [7] P. Roberson, T. King, R. Kunselman, J. Miller, R.J. Powers, P.D. Barnes, R.A. Eisenstein, R.B. Sutton, W.C. Lam, C.R. Cox, M. Eckhouse, J.R. Kane, A.M. Rushton, W.F. Vulcan and R.E. Welsh, Phys. Rev. **C5**, 1954 (1977).
- [8] Th. Köhler, P. Blüm, G. Büche, A.D. Hancock, H. Koch, A. Kreissl, H. Poth, U. Raich, D. Rochmann, G. Backenstoss, Ch. Findeisen, J. Repond, L. Tauscher, A. Nilsson, S. Carius, M. Suffert, S. Charalambus, M. Chardalas, S. Dedoussis, H. Daniel, T. von Egidy, F.J. Hartmann, W. Kanert, G. Schmidt, J.J. Reidy, M. Nicholas and A. Wolf, Phys. Lett. **B176**, 327 (1986).
- [9] D. Rohmann *et al.*, Z. Phys. **A325**, 261 (1986).
- [10] H.J. Körner and J.P. Schiffer, Phys. Rev. Lett. **27**, 1457 (1971).
- [11] C.J. Batty, Nucl. Phys. **A372**, 433 (1981).
- [12] C.J. Batty, Phys. Lett. **B189**, 393 (1987).
- [13] E. Friedman and J. Lichtenstadt, Nucl. Phys. **A455**, 573 (1986).
- [14] The CERN proposal, Experiment PS 209.
- [15] J. Cugnon and J. Vandermeulen, Ann. Phys. (Paris) **14**, 49 (1989).
- [16] P. Armanteros *et al.*, CERN/PSCC/80-101,1980.
- [17] H.R. Clover, R.M. DeVries, N.J. DiGiacomo, and Y. Yariv, Phys. Rev. **C26**, 2138 (1982); J. Roy *et al.*, in *Proceedings of International Seminar on  $N\bar{N}$* , Syracuse, 1975, edited by T.E. Kaloropoulos.
- [18] A.M. Green and S. Wycech, Nucl. Phys. **A377**, 441 (1982).
- [19] T. Suzuki and H. Narumi, Nucl. Phys. **A426**, 413 (1984).
- [20] S. Adachi and H.V. von Geramb, Acta Phys. Aust. **XXXVII**, 627 (1985); Nucl. Phys. **A470**, 461 (1987).
- [21] O. Dumbrajs, H. Heiselberg, A.S. Jensen, A. Miranda, G.C. Oades, and J.M. Richard, Nucl. Phys. **A457**, 491 (1986).
- [22] J. Kronenfeld, A. Gal, and J.M. Eisenberg, Nucl. Phys. **A430**, 413 (1984).
- [23] A.M. Green and S. Wycech, Nucl. Phys. **A467**, 744 (1987).
- [24] X. Campi and A. Bouyssy, Phys. Lett. **73B**, 263 (1978).
- [25] H. Bethe and Ph. Siemens, Nucl. Phys. **B21**, 587 (1970).
- [26] S. Wycech, F.J. Hartmann, H. Daniel, W. Kanert, H.S. Plendl, T. von Egidy, J.J. Reidy, M. Nicholas, L.A. Redmond, H. Koch, A. Kreissl, H. Poth, and D. Rohmann, Nucl. Phys. **A561**, 607 (1993).
- [27] L.C. Liu and C.M. Shakin, Phys. Lett. **B78**, 389 (1978).
- [28] J.N. Ginocchio, Phys. Rev. **C17**, 195 (1978).
- [29] R. Bizzari, P. Guidoni, F. Marcelija, F. Marzano, E. Castelli, M. Sessa, Nuovo Cim. **22A**, 225 (1974); T.E. Kalogeropoulos, Phys. Rev. **D22**, 2585 (1980).
- [30] D. Ashery, Nucl. Phys. **A355**, 385 (1980); D. Ashery, I. Navon, G. Azuleos, H.K. Walter, H.J. Pfeifer and F.W. Schlepütz, Phys. Rev. **C23**, 2173 (1981).

- [31] J.P. Shiffer, Nucl. Phys. **A355**, 339 (1980).
- [32] F. Balestra *et.al.*, Nucl. Phys. **A491**, 572 (1989).
- [33] N.N. Bogolyubov, JETP (Sov. Phys.) **7**, 41 (1958); Sov. Phys. Usp. **2**, 236 (1959); Usp. Fiz. Nauk **67**, 549 (1959).
- [34] P. Ring and P. Schuck, *The nuclear many-body problem* (Springer-Verlag, New York 1980).
- [35] J. Dobaczewski, H. Flocard, and J. Treiner, Nucl. Phys. **A422**, 103 (1984).
- [36] G.R. Satchler and W.G. Love, Phys. Reports **C55**, 183 (1979).
- [37] Y. Eisenberg and D. Kessler, Phys. Rev. **130**, 2352 (1961); A.D. Martin, Nuovo Cim. **27**, 1359 (1963); M. Leon and R. Seki, Phys. Rev. Lett. **32**, 132 (1973).
- [38] J.A. Wheeler, *Handbook of Physics*, edited by Condon and Odishow, (McGraw-Hill Book Comp., 1958), p.177.

TABLE I. Atomic results. Column 2 contains the principal q-number  $n$  and the angular momentum  $l$ . For the remaining columns: c.p. is the nuclear capture probability calculated under the assumption that the circular atomic state  $n = n_{\text{upper}} + 1$  is fully occupied,  $\sigma_{A-1} = \Gamma^{A-1}/\Gamma^{\text{tot}}$  is the branching ratio for the cold capture and  $\sigma_{np} = \Gamma_n/\Gamma_p$  is the ratio of captures on neutrons to protons. The AD model and  $R_{np} = 0.63$  were used.

ELEMENT	n	l	c.p.	$\sigma_{A-1}$	$\sigma_{np}$
$^{58}\text{Ni}$	4	3	0.	0.095	0.69
	5	4	0.16	0.097	0.69
	6	5	0.83	0.110	0.70
	7	6	0.01	0.150	0.71
	8	7	0.	0.220	0.71
$^{96}\text{Zr}$	6	5	0.24	0.106	4.67
	7	6	0.72	0.128	5.30
$^{130}\text{Te}$	7	6	0.05	0.096	1.77
	8	7	0.93	0.122	2.00
$^{144}\text{Sm}$	7	6	0.01	0.075	1.39
	8	7	0.75	0.085	1.46
$^{154}\text{Sm}$	7	6	0.01	0.087	3.65
	8	7	0.75	0.099	3.98
$^{176}\text{Yb}$	8	7	0.23	0.097	3.34
	9	8	0.75	0.124	4.07
$^{232}\text{Th}$	7	6	0.	0.073	3.94
	8	7	0.	0.091	4.64
	9	8	0.31	0.098	5.00
	10	9	0.69	0.127	6.20
$^{238}\text{U}$	9	8	0.29	0.106	6.55
	10	9	0.71	0.138	8.24

TABLE II. Comparison of nuclear models. Experimental and calculated results for  $\sigma_{A-1}$  and  $\sigma_{np}$  are given. Calculations for atomic orbitals weighted as in Table I are done with  $R_{np} = 0.82$ .

	Exp. [1]		AD		HF		HFB	
	$\sigma_{A-1}$	$\sigma_{np}$	$\sigma_{A-1}$	$\sigma_{np}$	$\sigma_{A-1}$	$\sigma_{np}$	$\sigma_{A-1}$	$\sigma_{np}$
$^{58}\text{Ni}$	0.098(8)	0.9(1)	0.11	0.90	0.110	0.785	0.110	0.781
$^{96}\text{Zr}$	0.161(22)	2.6(3)	0.12	4.9	0.125	2.54	0.117	2.40
$^{96}\text{Ru}$	0.113(17)	0.8(3)	0.10	1.7	0.099	0.944	0.099	0.955
$^{130}\text{Te}$	0.184(36)	4.1(1)	0.12	2.6	0.124	3.14	0.123	3.22
$^{144}\text{Sm}$	0.117(20)	< .4	0.09	1.9	0.094	1.38	0.092	1.36
$^{154}\text{Sm}$	0.121(20)	2.0(3)	0.10	5.1	0.110	3.34	0.106	2.96
$^{176}\text{Yb}$	0.241(40)	8.10(7)	0.12	4.8	0.111	3.23	0.109	3.50
$^{232}\text{Th}$	0.095(14)	5.4(8)	0.12	7.6	0.087	3.80	0.109	4.65
$^{238}\text{U}$	0.114(9)	6.0(8)	0.13	10	0.092	4.09	0.100	4.31

FIG. 1. The total antiproton absorption densities from the "upper"  $n = 6$ ,  $l = 5$  orbit in  $^{58}\text{Ni}$ :  $W_l$  for the  $N\bar{N}$  annihilation range  $r_0 = 1$  fm and  $W_s$  for the range  $r_0 = 0.75$  fm. The dot-dashed line is a ratio of two  $W_l$  for subsequent circular  $n = 5$  and  $n = 6$  atomic states.  $\rho_0$  is a "bare" neutron density. Normalisations are arbitrary.

FIG. 2. The  $(A - 1)$  "cold" antiproton absorption density on a neutron from  $n = 6$  circular orbit in  $^{58}\text{Ni}$ .  $A_l$  given by the integrand of Eq.(4) for the  $N\bar{N}$  annihilation range  $r_0 = 1$  fm and  $A_s$  for the range  $r_0 = 0.75$  fm.  $\rho_0$  is a "bare" neutron density. Normalisations are arbitrary. Missing probabilities (left scale):  $P_{\text{miss}}$  continuous is due to phase space alone,  $P_{\text{miss}}$  dash-dotted is calculated with corrections for the experimental pion momentum distribution. The flat dashed curve is  $P_{\text{dh}}$  from the HFB model.

FIG. 3. The ratios of neutron and proton densities calculated with several nuclear models in the  $^{144}\text{Sm}$  nucleus. Dashed line-HF, dotted-SP, dot dashed-AD, continuous line-HFB. The  $(A - 1)$  "cold" absorption density peaks at 8.6 fm marked with a dot while its bulk is located between 7.2 and 10.2 fm. The experimental  $\sigma_{np} < 0.4$ .

